

Phase-shifting interferometry with genetic algorithm-based twin image noise elimination

Joonku Hahn, Hwi Kim, Seong-Woo Cho, and Byoung-ho Lee*

School of Electrical Engineering, Seoul National University, Gwanak-Gu Sillim-Dong, Seoul 151-744, Korea

*Corresponding author: byoung-ho@snu.ac.kr

Received 9 May 2008; revised 3 July 2008; accepted 3 July 2008;
posted 7 July 2008 (Doc. ID 95981); published 25 July 2008

Phase-shifting interferometry with a genetic algorithm is proposed. The correction of unknown phase-shifting error is an important task in general phase-shifting interferometry. Since phase-shifting errors generate twin image noise in a reconstructed image, we can reduce the phase-shifting errors indirectly by trying to eliminate the twin-image noise in the reconstructed image. By Zernike polynomial expansion, the reconstructed image is represented as the evenness and oddness, where the ratio of the evenness and oddness is a measure of the amount of the twin image noise. We employ the genetic algorithm for finding the fittest phase shifts of interferograms by reducing the evenness of the reconstructed image, which leads to reduction of phase-shifting errors. This phase-shifting interferometry with a genetic algorithm is confirmed experimentally. © 2008 Optical Society of America

OCIS codes: 070.2580, 090.1760, 230.6120.

1. Introduction

Phase-shifting interferometry is a representative temporal phase measurement technology. This technology receives much attention not only to acquire three-dimensional information of objects, but also to measure the deformations or resonant stationary waves of instruments [1–4]. In general phase-shifting interferometry, at least three phase-shifting steps are required in order to delete nondiffractive terms and to remove any ambiguities of phases in the object wave. For the purpose of measuring the object wave accurately, the phase of the reference wave should be shifted definitely. However, practically, it is hard to avoid phase-shifting errors since both miscalibration and vibration of optics could cause phase-shifting errors [5].

The simplest approach to reduce the effect of phase-shifting errors is to simply increase the number of phase-shifting steps to more than three [6]. Phase-shifting interferometry with five steps is reported to be more robust than the method with four steps to the errors induced from linear phase-shift miscali-

bration and detector nonlinearity [7]. As branches of minimum-norm methods, the least-squares fitting method and the maximum-minimum algorithm present proper solutions in spite of phase-shifting errors [8,9]. However, these methods require a lot of phase-shifting steps to correct even one imprecise phase shift. And these are based on the pixel-by-pixel calculation among interferograms to evaluate the error function. If noises are randomly distributed in interferograms, these methods with pixel-by-pixel calculations cannot lead to optimized solutions.

To compensate these randomly distributed noises, integral methods averaging out whole phases in each interferogram are proposed. One integral method using a polynomial expansion in interferograms detects harmonic contents and deletes white Gaussian noise [10]. Other methods computing the averaged difference of phases among interferograms estimate arbitrary unknown phase shifts [11–13]. However, these integral methods assume that the average value of noises over each interferogram is quite small in comparison with its phase shift. And these evaluate the amounts of phase-shifting errors by computing interferograms on the hologram plane without taking reconstructed images into consideration.

Therefore, in the case that the noises distributed on interferograms cancel one another and their average is negligible, these methods cannot find the fittest solutions for improving reconstructed images.

As an indirect approach to error reduction, there are some methods that improve reconstructed images. In the case that the impulse response of the system is blurred resulting from the aberration, the sharpness metrics make the objects recognizable effectively [14–16]. However, this approach only focuses on eliminating annoying noise in reconstructed images by image processing. Therefore, it is impossible to find the amounts of phase-shifting errors quantitatively with these methods.

In this paper, we propose a novel scheme of phase-shifting interferometry with a genetic algorithm exploiting the special property of twin image phenomena, which frequently occur resulting from the inaccuracy of the phase shifter. The twin image noise in reconstructed images is a well known issue in digital holography. This twin image noise is a conjugate term of the object wave, where the conjugate term is regarded as the wave propagating in pseudo-coordinates from the hologram plane [17,18]. In general phase-shifting interferometry, phase-shifting errors lead to generating of twin image noise, and the degree of twin image noise is defined as a measure of the amount of phase-shifting errors. Therefore we can reduce the phase-shifting errors indirectly by trying to eliminate the twin-image noise in reconstructed images. The degree of twin image noise is evaluated by the ratio of coefficients in Zernike polynomials. Generally, Zernike polynomial expansion is used to express the aberration of optics [19]. The Zernike polynomials are composed of two-dimensional radial even and odd functions. These radial even and odd function sets are very useful for evaluating the existence and amount of twin image noise. The genetic algorithm is employed to find the optimized phases of interferograms to increase the oddness of the reconstructed image, that is, to eliminate the twin image noise.

This paper is organized as follows. In Section 2, the twin image noise in Fourier optics is expressed numerically. In Section 3, a genetic algorithm for eliminating twin image noise is proposed. In Section 4, experimental results are presented and discussed. In Section 5, a conclusion and perspective are given.

2. Twin Image Noise in Fourier Optics

In this section, general phase-shifting interferometry is explained, and the relation of twin image noise and phase-shifting errors is formulated. The characteristics of this twin image noise are described in Fourier optics, and from the resultant phase-shifting equation, how to estimate phase shifts of interferograms is detailed.

Figure 1 shows the optical configuration for phase-shifting interferometry in Fourier optics. The phase shifter is realized by the piezo-driven mirror, and the variable beam splitter is used to balance the inten-

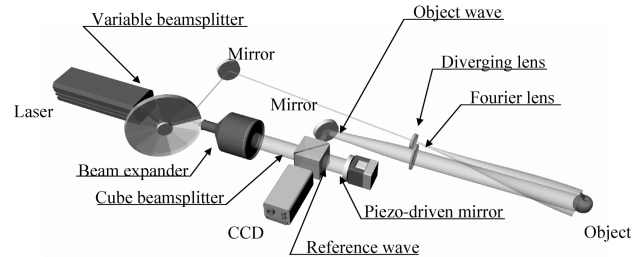


Fig. 1. Optical configuration for phase-shifting interferometry in Fourier optics.

sities of object and reference waves. This study is carried out in Fourier optics, which is preferred since the object wave is transformed by a Fourier lens. Therefore the broad angular spectrum is recorded in holograms, and the optical power loss of object waves is relatively small [20].

In general phase-shifting interferometry, the i th-step interferogram is represented as

$$I_i = |U_O + U_{R,i}|^2 = A_O^2 + A_R^2 + 2A_O A_R \cos(\varphi - \alpha_i), \quad (1)$$

where the object wave and reference wave are respectively given by

$$U_O = A_O \exp(j\varphi), \quad (2a)$$

$$U_{R,i} = A_R \exp(j\alpha_i). \quad (2b)$$

The relationship among phases of interferograms is easy to understand when interferograms are represented as two-dimensional vectors in the complex plane [21]. The unit vectors of the object wave and reference wave are defined by

$$\hat{\varphi} \equiv \exp(j\varphi) = (\cos \varphi, \sin \varphi), \quad (3a)$$

$$\hat{\alpha}_i \equiv \exp(j\alpha_i) = (\cos \alpha_i, \sin \alpha_i). \quad (3b)$$

And the i th-step interferogram is clearly represented as

$$I_i = A_O^2 + A_R^2 + 2A_O A_R \hat{\varphi} \cdot \hat{\alpha}_i. \quad (4)$$

Here the operator “ \cdot ” means inner product in the complex plane.

The difference between a pair of interferograms eliminates nondiffractive terms, and in this difference, the influence of the reference wave is removed by dividing with the amplitude of the reference wave. Therefore this result, I_{ij} , determined from a pair of interferograms and the amplitude of reference wave,

could be a base of phase-shifting interferometry, which is represented as

$$I_{ij} \equiv (I_i - I_j)/A_R = 2A_O \hat{\phi} \cdot (\hat{\alpha}_i - \hat{\alpha}_j) = 2A_O \sqrt{2 - 2 \cos(\alpha_i - \alpha_j)} \sin\left(\varphi - \frac{\alpha_i + \alpha_j}{2}\right). \quad (5)$$

This relation between two phases of interferograms in the complex plane is shown in Fig. 2. The norm of $(\hat{\alpha}_i - \hat{\alpha}_j)$ depends on the angle between $\hat{\alpha}_i$ and $\hat{\alpha}_j$ [22], and it is related to the influencing power of the base I_{ij} .

Most phase-shifting interferometry equations could be represented as the summation of the base I_{ij} with complex coefficients. For example, the four-step phase-shifting interferometry equations in class A of Ref. [7] are converted as follows:

$$-\tan(\varphi') = \frac{I_2 - I_4}{I_1 - I_3}, \quad (6a)$$

$$-\tan(\varphi' + \pi/4) = \frac{I_1 + I_2 - I_3 - I_4}{I_1 - I_2 - I_3 + I_4}, \quad (6b)$$

$$U'_O = I_{13} + jI_{42}, \quad (6c)$$

$$U'_O = e^{-\pi/4}(I_{12} + I_{43}) + je^{-\pi/4}(I_{31} + I_{42}). \quad (6d)$$

Here, prime means the calculated value from measured interferograms, and Eqs. (6a) and (6b) are equivalent to Eqs. (6c) and (6d), respectively.

In this paper, we use the phase-shifting interferometry equation without constraints that the coefficients are unities. Since any phase-shift base I_{ij} is represented as the summation of I_{i1} and $-I_{j1}$, without the loss of generality the phase-shifting interferometry equation is simplified as

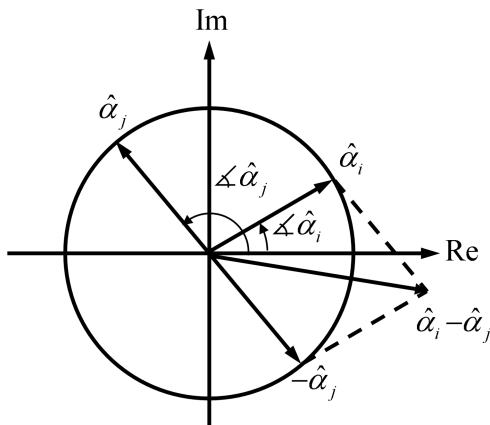


Fig. 2. Relation between two phases of interferograms in the complex plane.

$$U'_O = \sum_{i \neq 1} a_{i1} I_{i1}, \quad (7)$$

where a_{i1} is the complex number with the magnitude equal to or less than unity.

This phase-shifting interferometry equation is extended with the actual object wave term and the conjugate term as

$$\begin{aligned} U'_O &= \sum_{i \neq 1} 2a_{i1} A_O [(\cos \alpha_i - \cos \alpha_1) \cos \varphi \\ &\quad + (\sin \alpha_i - \sin \alpha_1) \sin \varphi] \\ &= \sum_{i \neq 1} a_{i1} [(\cos \alpha_i - \cos \alpha_1)(U_O + U_O^*) \\ &\quad + (\sin \alpha_i - \sin \alpha_1)(U_O - U_O^*)] \\ &= \sum_{i \neq 1} a_{i1} (\cos \alpha_i - \cos \alpha_1 + \sin \alpha_i - \sin \alpha_1) U_O \\ &\quad + \sum_{i \neq 1} a_{i1} (\cos \alpha_i - \cos \alpha_1 - \sin \alpha_i + \sin \alpha_1) U_O^*. \end{aligned} \quad (8)$$

Here, the actual object wave is given by U_O , and its conjugate U_O^* represents the twin image noise. The coefficient of U_O^* diminishes when phase shifts $\{\alpha_i | i \neq 1\}$ are definitely executed suitable for complex coefficients $\{a_{i1} | i \neq 1\}$. The phase-shift errors obstruct elimination of the twin image noise term in Eq. (8). Therefore there is a close connection between the twin image noise and phase-shifting errors, and the degree of twin image noise could be a measure of the amount of phase-shifting errors.

In this paper the hologram is located at the focal plane, and the propagation of twin image noise in Fourier optics is explained as the transfer function. In a hologram with Fourier optics the original object image and twin image noise are spatially related to each other. Figure 3 shows the schematic of a hologram with a Fourier transform lens with focal length f . The propagation of an actual object wave from $z = z_0$ to the backward focal plane $z = 2f$ is formulated as

$$U_O(\lambda f f_X, \lambda f f_Y; z = 2f) = H(f_X, f_Y; z_0) \mathbf{F}[U_O(x, y; z_0)]. \quad (9)$$

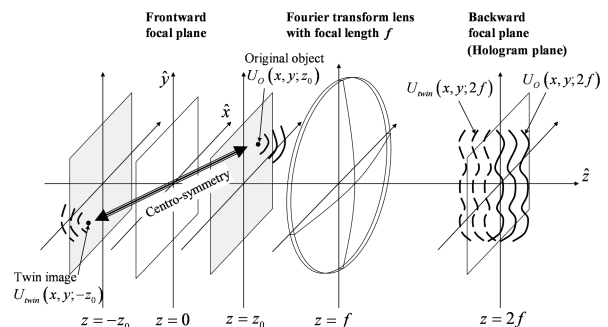


Fig. 3. Original object and twin image in hologram with Fourier optics.

Here, \mathbf{F} denotes Fourier transform and $H(f_X, f_Y; z_0)$ is the transfer function, defined as

$$H(f_X, f_Y; z_0) = \frac{A}{j\lambda f} \exp[j\pi\lambda z_0(f_X^2 + f_Y^2)]. \quad (10)$$

And, the conjugate of this transfer function is represented as

$$H^*(f_X, f_Y; z_0) = -H(f_X, f_Y; -z_0). \quad (11)$$

Therefore the propagation of twin image noise is given by

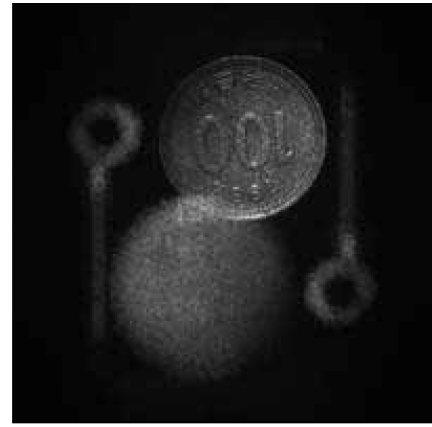
$$\begin{aligned} U_{\text{twin}}(x, y; -z_0) &= \mathbf{F}^{-1}[U_O^*(\lambda f f_X, \lambda f f_Y; z = 2f) / \\ &\quad H(f_X, f_Y; -z_0)] \\ &= -\mathbf{F}^{-1}\{[U_O(-\lambda f f_X, -\lambda f f_Y; z = 2f) / \\ &\quad H(-f_X, -f_Y; z_0)]^*\} \\ &= -U_O^*(-x, -y; z_0). \end{aligned} \quad (12)$$

In Eq. (12), the twin image appears centrosymmetrically with the original object image at the reconstruction plane, and Fig. 4 shows this characteristic from experimental results where the images are numerically reconstructed at various positions. The hologram is constructed with a single base, and there is an ambiguity of π , which leads to the existence of twin image noise with the same intensity as the actual object wave. Bolts are located at the focal plane $z = 0$, and a coin is located at $z = 0.2f$. Both twin and original object images of the bolts are in focus at $z = 0$, as shown in Fig. 4(b). On the other hand, in the case of the coin, the twin image is in focus at $z = -0.2f$ in Fig. 4(a), and the original object image is in focus centrosymmetrically at $z = 0.2f$ in Fig. 4(c).

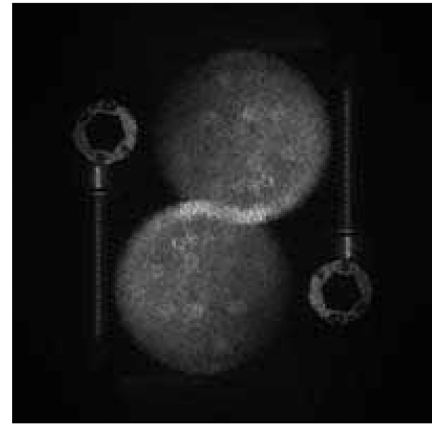
The centrosymmetric property of twin image noise makes the reconstructed image be centrosymmetric when the twin image noise exists. Therefore the existence of the centrosymmetry in a reconstructed image can be a criterion for phase-shifting error. In this paper, we evaluate the centrosymmetry in a reconstructed image to solve the unknown phase shifts. Even though this technique is not applicable when the original object has perfect centrosymmetry and is positioned on the optical axis, this is evitable by shifting the original object off the optical axis. This shift removes the centrosymmetry in the reconstructed image with the original object, but the clear separation between the original object image and twin image noise is unnecessary. In Section 4, we present some interesting cases that the evaluation of the centrosymmetry is very effective for finding the proper solutions of unknown phase shifts.

3. Genetic Algorithm for Eliminating Twin Image Noise

In this section, the genetic algorithm for eliminating twin image noise using a Zernike expansion is described. The degree of the twin image is evaluated by the evenness of the reconstructed image with



(a)



(b)



(c)

Fig. 4. Numerical reconstructions of twin images in Fourier optics at (a) $z = -0.2f$, (b) $z = 0$, and (c) $z = 0.2f$.

the help of a Zernike expansion, and the coefficients of phase-shift bases are optimized genetically.

The original object image and its twin image in Fourier optics have the centrosymmetric relation at the forward focal plane. If the original object image and the twin image have equal intensities, the reconstructed image can be expanded with two-dimensional even functions. Therefore the evenness of the reconstructed image reflects the degree of the

twin image noise, and, as previously discussed, the vanishing of the twin image means the diminution of phase-shifting errors. Zernike polynomials expansion is useful to evaluate the evenness and oddness in a reconstructed image. In general, Zernike polynomials are applied to express the two-dimensional aberration composed of even and odd functions. With the normalization conditions, the real Zernike polynomials could be redefined as

$$U_n^m \equiv \begin{cases} \sqrt{(n+1)/\pi} R_n^0(\rho), & m = 0 \\ \sqrt{2(n+1)/\pi} R_n^m(\rho) \cos m\theta, & m > 0, \\ -\sqrt{2(n+1)/\pi} R_n^{-m}(\rho) \sin m\theta, & m < 0 \end{cases} \quad (13)$$

where ρ and θ refer to cylindrical coordinates. Here, radial polynomials $R_n^{\pm m}(\rho)$ are defined as

$$R_n^{\pm m}(\rho) = \sum_{s=0}^{(n-m)/2} (-1)^s \times \frac{(n-s)!}{s!((n+m)/2-s)!((n-m)/2-s)!} \rho^{n-2s}. \quad (14)$$

These real Zernike polynomials are classified into even and odd functions according to the number m . The real Zernike polynomials with even number m are even functions, and the real Zernike polynomials with odd number m are odd functions.

We define the cost function of a genetic algorithm by evaluating the degree of twin image noise as the sum of even coefficients over the sum of odd coefficients:

$$\text{cost function} = - \frac{\sum_n \sum_{m=0, \pm 2, \pm 4, \dots, \pm n} (\text{coefficients of } U_n^m)}{\sum_n \sum_{m=\pm 1, \pm 3, \dots, \pm n} (\text{coefficients of } U_n^m)}. \quad (15)$$

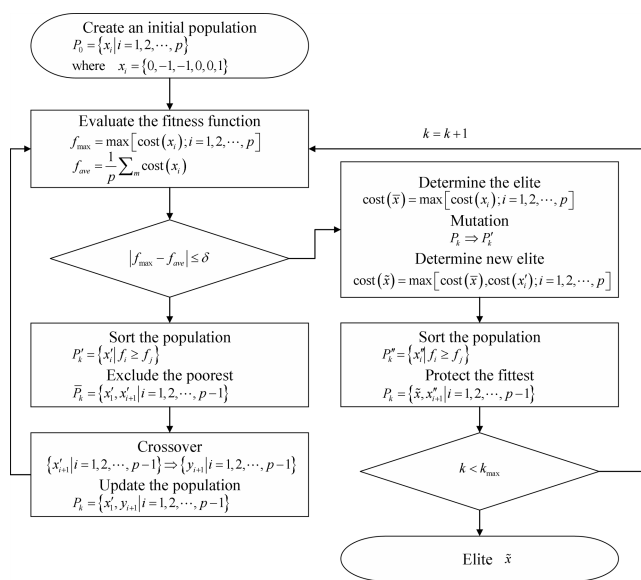
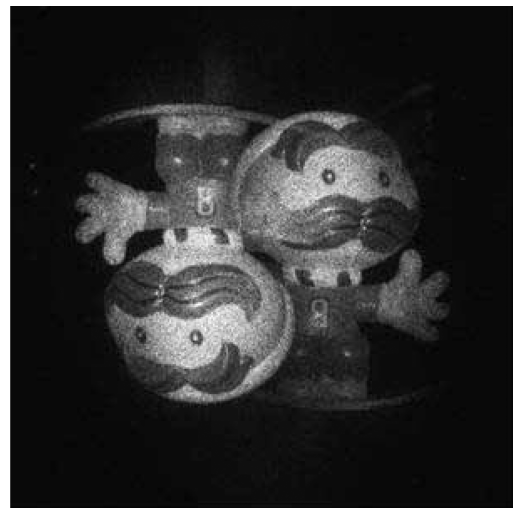


Fig. 5. Flow of the microgenetic algorithm to eliminate a twin image.

If the twin image is diminished, the sum of even coefficients decreases down to the sum of odd coefficients, and the cost function is close to negative one. In this paper, we calculate the cost function with the real Zernike polynomials up to $n = 8$.

The genetic algorithm searches local optima through two distinguished operations, which are mutation and crossover [23]. The mutation is simply a random search and makes small variations of the present solution. The crossover operation is proper in the convex optimization problem since the crossover operation is mathematically analogous to the linear combination of two chromosomes in the floating point coding scheme. The optimization of coefficients in the linear combination of phase-shift bases is a typical convex problem. In this paper, we use the microgenetic algorithm including the subloop of crossover operations to search the optimized

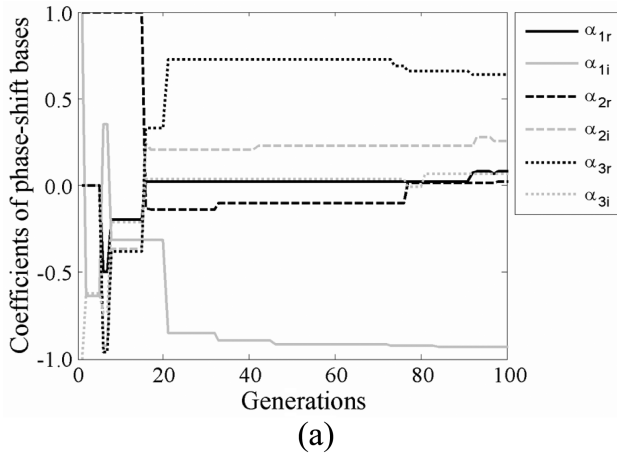


(a)

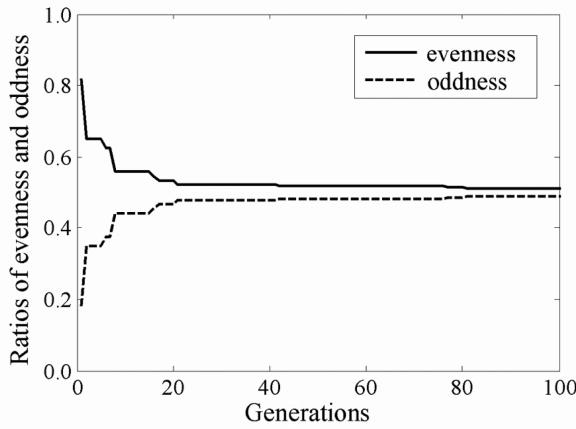


(b)

Fig. 6. Numerically reconstructed images (a) before and (b) after the genetic algorithm.



(a)



(b)

Fig. 7. Evolutions in the genetic algorithm of (a) the fittest chromosome and (b) the resultant evenness and oddness in reconstructed images.

solutions efficiently. Figure 5 shows the flow of this microgenetic optimization.

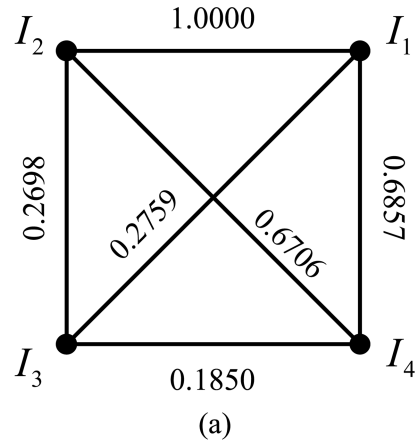
The chromosome in this microgenetic algorithm is composed of the coefficients in Eq. (7), which is defined as

$$x_i = \{\text{Re}\{a_{21}\}, \text{Im}\{a_{21}\}, \text{Re}\{a_{31}\}, \text{Im}\{a_{31}\}, \dots, \text{Re}\{a_{N1}\}, \text{Im}\{a_{N1}\}\}. \quad (16)$$

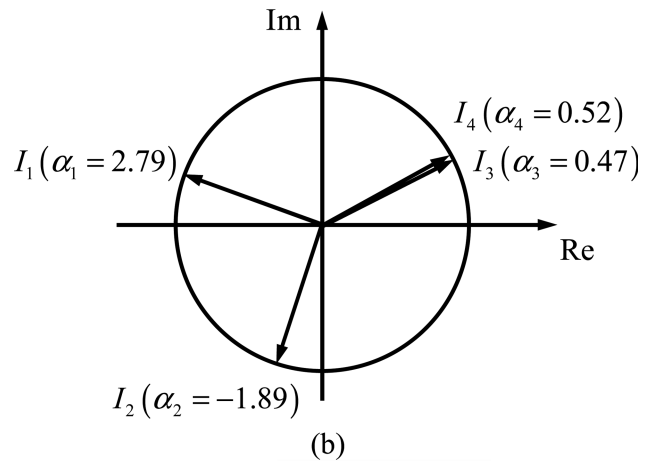
In this paper, the number of phase-shifting steps is four, which is a proper number that explains the relationship among phase-shift bases in connection with phase shifts of interferograms. At the first generation, the chromosome is set following the coefficients of the phase-shift bases in a conventional four step algorithm, like

$$x_i = \{0, -1, -1, 0, 0, 1\}. \quad (17)$$

After optimization, resultant phase shifts of interferograms can be estimated. The optimized object wave in the phase-shifting interferometry equation, Eq. (7), is represented as



(a)



(b)

Fig. 8. Relationship between (a) the optimized coefficients of phase-shift bases and (b) the resultant phase shifts of interferograms.

$$U'_O = \sum_{i \neq 1} 2a_{i1}A_O[(\cos \alpha_i - \cos \alpha_1) \cos \varphi + (\sin \alpha_i - \sin \alpha_1) \sin \varphi]. \quad (18)$$

The error function between the actual object wave and the optimized object wave is defined as

$$e = |U'_O - cU_O| = \left| \sum_{i \neq 1} 2a_{i1}A_O[(\cos \alpha_i - \cos \alpha_1) \cos \varphi + (\sin \alpha_i - \sin \alpha_1) \sin \varphi] - c(\cos \varphi + j \sin \varphi) \right|. \quad (19)$$

Here, the constant c is a factor to balance the magnitudes of them. Since there are enormous numbers of pixels in an interferogram and the phase φ is distributed uniformly, we assume that the phase φ is an arbitrary independent value. Therefore the variables $\cos \varphi$ and $\sin \varphi$ in the spatial average of the error function could be treated as being independent columns, and real and imaginary values could be regarded as independent rows,

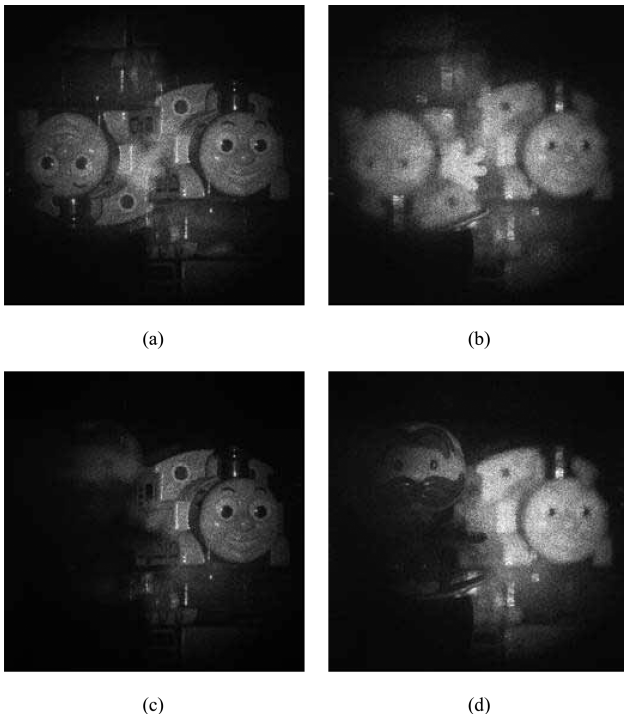


Fig. 9. Numerically reconstructed images. Parts (a) and (b) show the images at the focal plane $z = 0$ and defocused plane $z = 0.2f$, respectively, before the optimization. Parts (c) and (d) show the images at the same positions as (a) and (b) after the optimization.

$$\begin{aligned}
 \langle e \rangle &= \langle |U'_O - cU_O| \rangle \\
 &= \text{norm} \left(\begin{pmatrix} \text{Re}\{a_{21}\} & \text{Re}\{a_{31}\} & \cdots & \text{Re}\{a_{N1}\} \\ \text{Im}\{a_{21}\} & \text{Im}\{a_{31}\} & \cdots & \text{Im}\{a_{N1}\} \end{pmatrix} \right) \\
 &\times \begin{pmatrix} \cos\alpha_2 - \cos\alpha_1 & \sin\alpha_2 - \sin\alpha_1 \\ \cos\alpha_3 - \cos\alpha_1 & \sin\alpha_3 - \sin\alpha_1 \\ \vdots & \vdots \\ \cos\alpha_N - \cos\alpha_1 & \sin\alpha_N - \sin\alpha_1 \end{pmatrix} - c \begin{pmatrix} 1 & 0 \\ 0 & 1 \end{pmatrix} \right), \quad (20)
 \end{aligned}$$

where the angle bracket $\langle \cdot \rangle$ means the spatial average of waves, and the function $\text{norm}(\cdot)$ of a matrix is defined as a scalar that measures the magnitude of the elements in the matrix. In Eq. (20), there are four equations and $(N + 1)$ unknown variables, which are $\alpha_1, \alpha_2, \dots, \alpha_N$, and c . Therefore the resultant phase shifts, $\alpha_1, \alpha_2, \dots, \alpha_N$, are solved by minimizing the spatial average of the error, $\langle e \rangle$.

4. Experimental Results

In this section, experimental results are presented and discussed. From the interferometry with unknown phase shifts, the twin image noise is eliminated by the proposed genetic algorithm and the unknown phase shifts are estimated. By the use of the resultant hologram, the reconstructed images with a liquid crystal spatial light modulator (LC SLM) are presented.

In this paper, a Coherent Verdi 5 W Nd:YAG laser with a wavelength of 532 nm is used as a light source.

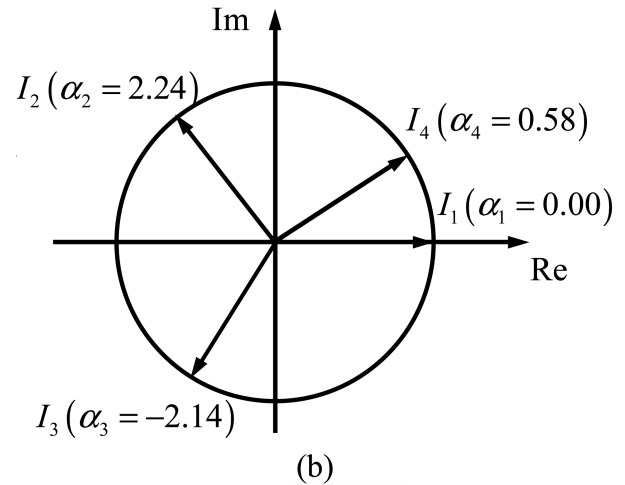
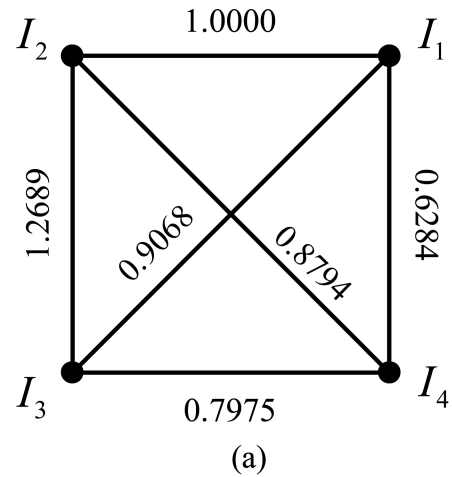


Fig. 10. Relationship between (a) the optimized coefficients of phase-shift bases and (b) the resultant phase shifts of interferograms.

We use an XYZ-38 made by Piezosystem Jena as the piezo stage for phase shifts and a KODAK MegaPLUS ES1.0/MV with 8 bit resolution as the CCD whose pixel size is $9\mu\text{m}$. The focal length of the Fourier lens is 750 mm. The CCD is located at the backward focal plane that is a hologram plane as previously mentioned in Fig. 3.

Figure 6 shows the numerically reconstructed images of the hologram with a plastic doll placed at the forward focal plane. In Fig. 6(a), the twin image appears definitely, but after processing with the proposed genetic algorithm, it is certainly lessened, as shown in Fig. 6(b). Figure 7 shows the evolutions in the genetic algorithm, where six variables of the fittest chromosome at each generation and the resultant evenness and oddness in reconstructed images are shown in Figs. 7(a) and 7(b), respectively. The evenness and oddness are enumerated as ratios of the sum of the coefficients in even-function and odd-function terms to their total sum. The evenness and oddness become close to each other as the twin image noise disappears as expected.

Figure 8 shows the relationship between the optimized coefficients of phase-shift bases and the resultant phase shifts of interferograms. In Fig. 8(a), the absolute value of a complex coefficient defined in Eq. (7) is noted between two related interferograms where the value is scaled with the absolute value of a_{21} being unity. For example, the absolute value of a_{41} , 0.6857, is presented between I_4 and I_1 . These absolute values stand for the contributions of related phase-shift bases defined in Eq. (7). Figure 7(b) shows phase shifts of interferograms. The third phase shift, α_3 , and the fourth phase shift, α_4 , are too close, and the contribution of the base I_{43} is relatively small as 0.1850. This relationship is a natural consequence since I_{43} has relatively little information of the object wave, as discussed in Section 2.

In our another experiment, one plastic doll is placed at the forward focal plane $z = 0$, and a plastic train is placed at the defocused plane $z = 0.2f$. Figures 9(a) and 9(b) show reconstructed images at the focal plane and defocused plane, respectively, before genetic optimization. In Fig. 9(b), the doll is indistinguishable, overlapped with the twin image noise of the train. However, after the optimization, the twin image noise disappears not only at the forward focal plane as shown in Fig. 9(c), but also at the defocused plane, and the doll is certainly distinguishable as shown in Fig. 9(d).

Figure 10 shows the relationship between the optimized coefficients of phase-shift bases and the resultant phase shifts of interferograms from the results shown in Fig. 9. Here, there exists the same relationship that the contribution of the base with a narrow phase-shifting angle between a pair of interferograms is small. That is, the phase shifts of two interferograms I_4 and I_1 are close to each other, and the contribution of phase shift base I_{41} is relatively small.

In these experimental results, the twin image noise is not clearly separated from the original object image, and the overlapped portion of twin image noise cannot be removed by simple blocking as the synthesis of one-side band Fourier transform hologram. However, the solution of phase shifts with a genetic algorithm eliminates the twin image noise effectively, and the portion of original object image overlapped with twin image noise is distinguishable.

Figure 11 shows the reconstructed images by LC SLM with previously discussed holograms. In this paper, we use an Epson L3P06X as the LC SLM with pixel size $12\ \mu\text{m}$ and a laser with wavelength 532 nm. Figures 11(a) and 11(b) are reconstructed images before genetic optimization and Figs. 11(c) and 11(d) are reconstructed images after the proposed genetic optimization. The comparison of two groups shows the distinct improvements in reducing twin image noises.

5. Conclusion

With the proposed phase-shifting interferometry, we can eliminate twin image noise and find the fittest solutions in coefficients of the phase-shift bases. In

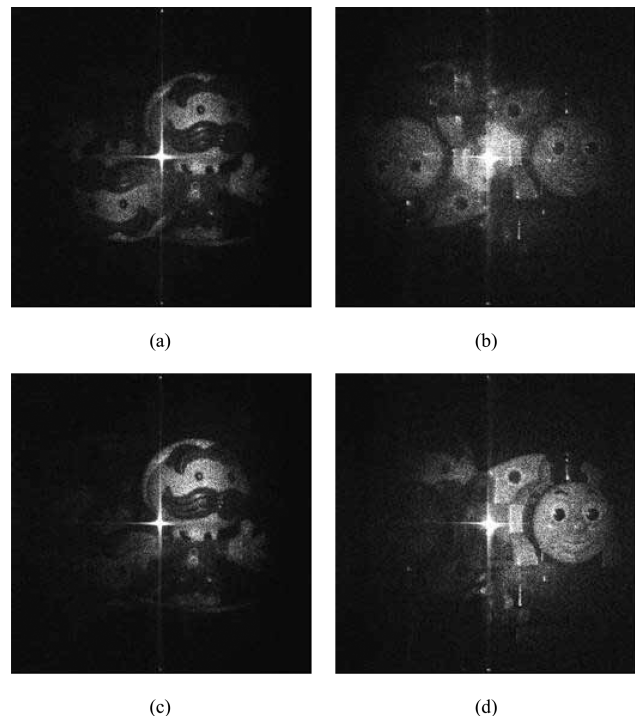


Fig. 11. Reconstructed images by LC SLM with previous holograms. Parts (a) and (b) are before the optimization and parts (c) and (d) are after the proposed optimization.

the reconstruction of a digital hologram from the measurement of phase-shift interferometry, the twin image noise is the result of phase-shifting errors, which is represented as a nonvanishing conjugate term. We can reduce the phase-shifting errors indirectly by trying to eliminate the twin image noise in the reconstructed images. In this paper, the degree of twin image noise was evaluated by the evenness in reconstructed images, and the genetic algorithm was applied to find the fittest solution of the object wave by controlling the coefficients of the phase-shift bases. The separation of the evaluation of twin image noise at the reconstruction plane and the construction of the object wave from phase-shift bases at the hologram plane gives more degrees of freedom than conventional methods. By encoding resultant holograms on a practical LC SLM, we showed that the outcomes agree with the numerically reconstructed images. It is expected that the proposed technique can be useful not only in the Fourier optics dealt with in this paper, but also in general Fresnel optics.

This work was supported by the Korea Science and Engineering Foundation and the Ministry of Education, Science, and Engineering of Korea through the National Creative Research Initiative Program (Active Plasmonics Applications Systems).

References

1. K. Creath, "Temporal phase measurement methods," in *Interferogram Analysis, Digital Fringe Pattern Measurement Tech-*

- niques, D. W. Robinson and G. T. Reid, eds. (Taylor & Francis, 1993), pp. 94–140.
2. I. Yamaguchi, "Phase-shifting digital holography," in *Digital Holography and Three-Dimensional Display*, T.-C. Poon, ed. (Springer, 2006), pp. 145–171.
 3. B. Y. Zel'dovich, A. V. Mamaev, and V. V. Shkunov, *Speckle Wave Interactions in Application to Holography and Nonlinear Optics* (CRC Press, 1995).
 4. J. Hahn, H. Kim, and B. Lee, "Optical implementation of iterative fractional Fourier transform algorithm," *Opt. Express* **14**, 11103–11112 (2006).
 5. L. Waller and G. Barbastathis, "Error analysis of phase-shifting for phase and amplitude tomographic reconstruction," in *Signal Recovery and Synthesis*, Technical Digest Series (OSA 2007), paper CTuB5.
 6. G. Lai and T. Yatagai, "Generalized phase-shifting interferometry," *J. Opt. Soc. Am. A* **8**, 822–827 (1991).
 7. J. Schmit and K. Creath, "Extended averaging technique for derivation of error-compensating algorithms in phase-shifting interferometry," *Appl. Opt.* **34**, 3610–3619 (1995).
 8. G.-S. Han and S.-W. Kim, "Numerical correction of reference phases in phase-shifting interferometry by iterative least-squares fitting," *Appl. Opt.* **33**, 7321–7325 (1994).
 9. X. Chen, M. Gramaglia, and J. A. Yeazell, "Phase-shifting interferometry with uncalibrated phase shifts," *Appl. Opt.* **39**, 585–591 (2000).
 10. A. Patil, R. Langoju, and P. Rastogi, "An integral approach to phase shifting interferometry using a super-resolution frequency estimation method," *Opt. Express* **12**, 4681–4697 (2004).
 11. L.-Z. Cai, Q. Liu, Y.-R. Wang, X.-F. Meng, and M.-Z. He, "Experimental demonstrations of the digital correction of complex wave errors caused by arbitrary phase-shift errors in phase-shifting interferometry," *Appl. Opt.* **45**, 1193–1202 (2006).
 12. L. Z. Cai, Q. Liu, and X. L. Yang, "Generalized phase-shifting interferometry with arbitrary unknown phase steps for diffraction objects," *Opt. Lett.* **29**, 183–185 (2004).
 13. X. F. Xu, L. Z. Cai, Y. R. Wang, X. L. Yang, X. F. Meng, G. Y. Dong, X. X. Shen, and H. Zhang, "Generalized phase-shifting interferometry with arbitrary unknown phase shifts: direct wave-front reconstruction by blind phase shift extraction and its experimental verification," *Appl. Phys. Lett.* **90**, 121124 (2007).
 14. J. R. Fienup and J. J. Miller, "Aberration correction by maximizing generalized sharpness metrics," *J. Opt. Soc. Am. A* **20**, 609–620 (2003).
 15. S. T. Thurman and J. R. Fienup, "Phase error correction for digital holographic imaging," in *Signal Recovery and Synthesis*, Technical Digest Series (OSA, 2007), paper SMC1.
 16. E. Cuche, P. Marquet, and C. Depeursinge, "Spatial filtering for zero-order and twin-image elimination in digital off-axis holography," *Appl. Opt.* **39**, 4070–4075 (2000).
 17. T.-C. Poon, T. Kim, G. Indebetouw, B. W. Schilling, M. H. Wu, K. Shinoda, and Y. Suzuki, "Twin-image elimination experiments for three-dimensional images in optical scanning holography," *Opt. Lett.* **25**, 215–217 (2000).
 18. J. Hahn, H. Kim, and B. Lee, "Optimization of the spatial light modulation with twisted nematic liquid crystals by a genetic algorithm," *Appl. Opt.* **47**, 2357 (2008).
 19. M. Born and E. Wolf, *Principles of Optics*, 7th ed. (Cambridge University Press, 1999).
 20. J. W. Goodman, *Introduction to Fourier Optics*, 3rd ed. (Roberts & Company, 2004).
 21. G. B. Arfken and H. J. Weber, *Mathematical Methods for Physicists*, 5th ed. (Academic, 2001).
 22. L. V. Ahlfors, *Complex Analysis*, 3rd ed. (McGraw-Hill, 1979).
 23. Z. Michalewicz, *Genetic Algorithms + Data Structures = Evolution Programs* (Springer-Verlag, 1999).